Crystallization Kinetics of Poly (L-lactic acid)/ Montmorillonite Nanocomposites Under Isothermal Crystallization Condition

Jiunn-Jer Hwang,[1] Su-Mei Huang,[1] Hsin-Jiant Liu,[2] Hawn-Chung Chu,[3] Li-Huei Lin,[2] Chen-Sheng Chung[2]

[1]*Department of Chemical Engineering, Army Academy, Chung-Li 320, Taiwan, Republic of China*
[2]*Department of Chemical and Materials Engineering, Vanung University, 1, Chung-Li 320, Taiwan, Republic of China*
[3]*Department of Chemical and Materials Engineering, Lee-Ming Institute of Technology, 2-2, Taishan, Taipei County, Taiwan, Republic of China*

Received 18 September 2010; accepted 14 July 2011
DOI 10.1002/app.35254
Published online 26 October 2011 in Wiley Online Library (wileyonlinelibrary.com).

ABSTRACT: Poly(L-lactic acid)/*o*-MMT nanocomposites, incorporating various amounts of organically modified montmorillonite (*o*-MMT; 0–10 wt %), were prepared by solution intercalation. The montmorillonite (MMT) was organically modified with dilauryl dimethyl ammonium bromide (DDAB) by ion exchange. Transmission electron microscopy (TEM) and X-ray diffraction (XRD) reveal that the *o*-MMT was exfoliated in a poly(L-lactic acid), (PLLA) matrix. A series of the test specimens were prepared and subjected to isothermal crystallization at various temperatures (T_1–T_5). The DSC plots revealed that the PLLA/*o*-MMT nanocomposites that were prepared under nonisothermal conditions exhibited an obvious crystallization peak and recrystallization, but neat PLLA exhibited neither. The PLLA/*o*-MMT nanocomposites (2–10 wt %) yielded two endothermic peaks only under isothermal conditions at low temperature (T_1), and the intensity of Tm_2 (the higher melting point) was proportional to the *o*-MMT content (at around 171°C). The melting point of the test samples increased with the isothermal crystallization temperature. In the Avrami equation, the constant of the crystallization rate (k) was inversely proportional to the isothermal crystallization temperature and increased with the *o*-MMT content, especially at low temperature (T_1). The Avrami exponent (n) of the PLLA/*o*-MMT nanocomposites (4–10 wt %) was 2.61–3.56 higher than that of neat PLLA, 2.10–2.56, revealing that crystallization occurred in three dimensions. J Appl Polym Sci 124: 2216–2226, 2012

Key words: poly(L-lactic acid); montmorillonite; nanocomposite; Avrami equation; crystalline formation

INTRODUCTION

Biomedical materials are important in various medical treatments that support rapid recovery with few side effects. Some biomaterials with low crystallinity and biodegradability that incorporate poly(lactic acid) are used as medical-fixed components with high absorbability, including bone screws, tacks, plates, and protective sheets. When they are implanted in the human body, they can be completely adsorbed by hydrolysis and react with citric acid. Finally, they are metabolized to yield carbon dioxide and water.

Poly(lactic acid) not only exhibits higher biodegradability and biocompatibility but also has favorable physical and mechanical properties. However, it has one great shortcoming, poor heat resistance, which limits its range of applications and commercial value. The degree of crystallinity of poly(lactic acid) strongly influences its mechanical and combinatorial properties.[1–4] Montmorillonite is extensively used as nanofillers to reinforce the scaffold, including acrylic fibers, epoxy resins, and polyimides.[5–7] Layered silicate nanofiller contains nanolayers and has high rigidity; it can limit the fluidity of polymeric chains, and thereby improve their thermal stability, mechanical strength, flame retardancy, and barrier property.[8–21] The several methods for preparing polymer/montmorillonite nanocomposites by the exfoliation or intercalation of *o*-MMT in the polymer matrix, usually using *in situ* polymerization, include solution polymerization, emulsion polymerization, suspension polymerization, polycondensation, and ring-opening polymerization. Other methods include melt intercalation.[22–24] To promote the compatibility of clay with polymers, the Na^+ and Ca^{2+} residing in the interlayer regions can be replaced by organic cations such as

Correspondence to: J.-J. Hwang (jiunnjer1@hotmail.com).
Contract grant sponsor: National Science Council of the Republic of China, Taiwan; contract grant number: NSC 95-2622-E-238-019-cc3.

alkylammonium ions via a cationic-exchange reaction to render the hydrophilic-layered silicate. This reaction also increases the spacing between the silicate layers, promoting the penetration of polymer chains or precursors into the spaces between them.[25–29]

The crystallization behavior of poly(L-lactic acid) in the presence of montmorillonite has been studied in our previous research. We found that the isothermal crystallization temperature dictated the morphology of the PLLA nanocomposites incorporating 2 wt % organophilic clay, that the phenomenon of recrystallization existed at lower isothermal crystallization temperature, and that the value of T_c of the PLLA/MMT nanocomposites increased, signifying the crystalline structure was more perfect, upon increasing the isothermal crystallization temperature.[30]

In this study, using similar method in our previous study, i.e., various quantities of *o*-MMT (0–10 wt %) were incorporated into poly(L-lactic acid) by solution intercalation and nanocomposite specimens were prepared under various isothermal crystallization conditions. The main objective of this article is to understand the effect of *o*-MMT content on the crystallization kinetics using the Avrami equation and the crystallization behavior of neat PLLA upon nanocomposite formation with *o*-MMT by differential scanning calorimetry (DSC) at various isothermal crystallization temperatures.

EXPERIMENTAL

Materials

PLLA (M_w 85,000–160,000 g mol^{-1}) was purchased from Bio Invigor. MMT [PK805; cation (Na^+) exchange capacity = 98 mequiv/100 g] was purchased from Paikong Nano Technology (Taipei, Taiwan). Dilauryl dimethyl ammonium bromide (DDAB; $[CH_3(CH_2)_{11}]_2(CH_3)_2NBr$) was purchased from TCI (Tokyo, Japan). Chloroform ($CHCl_3$) was obtained from Merck.

Modification of MMT

PK805 was treated with intercalating reagent (DDAB) using the ion exchange method. The amount of intercalating agent used was determined using the following equation.

$$98\,\text{mequiv}/100\,\text{g} \times W(\text{for clay}) \times 1.2 = (X/M_W\,\text{of intercalating agent}) \times 1 \times 1000$$

where 98 mequiv/100 g is the cation-exchange capacity per 100 g of MMT clay (PK805) and W is the quantity of clay used each time, 1.2 represents the excess intercalating agent used, X and M_W represents the quantity and molecular weight of the intercalating reagent, respectively.

MMT (5 g) was dispersed in 800 mL of deionized water and mixed for 24 h at room temperature. DDAB (2.5 g) was dissolved in 20 mL of deionized water, mixed for 1 h, and then slowly added to a saturated, swollen clay solution, which was agitated for 48 h at room temperature. The organically modified MMT was recovered by filtering the solution and then washing the filter cake with 900 mL deionized water to remove excess ions. The final product was dried at 100°C in a vacuum oven for 24 h. The dried, modified clay was then ground to a powder and passed through a 325-mesh sieve. The particle diameter of the resulting powder was around 40 μm.

Preparation of PLLA/*o*-MMT nanocomposites

PLLA was dried in a vacuum oven at 80°C for 12 h and stored in a desiccator at room temperature. The *o*-MMT was mixed at various ratios (2–10 wt %) with PLLA (3 g) in $CHCl_3$ (20 mL) and stirred for 24 h. The solution was then cast into film form and dried in a vacuum oven at 60°C for 24 h, before being stored in a desiccator.

METHODS

Wide-angle X-ray diffraction (WAXD)

A Thermo ARL X'tra X-ray diffractometer was used to obtain the X-ray diffraction (XRD) patterns of the samples. The X-ray beam was Ni-filtered Cu Kα radiation from a sealed tube. To calculate the *d*-spacing, Bragg's law was used:

$$n\lambda = 2d \sin\theta \quad (1)$$

where θ is the angle between the incident ray and the scattering planes, n is an integer that denotes the order (n = 1, 2, or 3), and λ is the wavelength (λ = 1.541 Å). The *o*-MMT and the PLLA/*o*-MMT nanocomposites were analyzed in a 2θ range of 1 to 60°; the scanning rate was 1.5° min^{-1} and the resolution was 0.05°.

Transmission electron microscopy (TEM)

The samples for TEM analysis were prepared by placing films of the PLLA/*o*-MMT nanocomposites into epoxy resin capsules and then curing the epoxy resin at 70°C for 24 h in a vacuum oven. The cured epoxy resins, containing the PLLA/*o*-MMT nanocomposites, were then microtomed using a Reichert-Jung Ultracut-E into 60- to 90-nm-thick slices. Subsequently, one layer of carbon (around 10-nm thick) was deposited on these slices on 100-mesh copper nets for TEM observation using a JEOL 2010 instrument operated at an accelerating voltage of 200 kV.

Differential scanning calorimetry (DSC)

A Perkin–Elmer series 6 differential scanning calorimetry was used to study the melting and crystallization behavior of the samples. The DSC experiments were performed with an N_2 flow rate of 20 mL min^{-1}. The nonisothermal crystallization procedure had comprised six stages:

1. Isothermal—the aluminum plate was placed in the DSC instrument for 1 min at 25°C to ensure thermal stability;
2. Temperature scan—the sample was heated from 25 to 190°C at a rate of 20°C min^{-1};
3. Isothermal—the temperature was maintained at 190°C for 2 min to eliminate the thermal history;
4. Temperature scan—the sample was cooled from 190 to 25°C at a rate of 1°C min^{-1};
5. Isothermal—the temperature was maintained at 25°C for 1 min to ensure thermal stability;
6. Temperature scan—the sample was heated from 25 to 190°C at a rate of 5°C min^{-1}.

The DSC thermal curve (cooling scan) under nonisothermal crystallization conditions was utilized to determine the isothermal crystallization temperature (T_1, T_2, T_3, T_4, or $T_{5)}$ of the samples. First, the curved upper portion was uniformly divided at the beginning of crystallization into five parts, and the three central parts were divided into five parts to obtain T_1–T_5. The isothermal crystallization procedure comprised six stages:

Stages 1–3 were as above.

4. Temperature scan—the sample was cooled from 190°C to the isothermal crystallization temperature (T_1, T_2, T_3, T_4, or $T_{5)}$ at a rate of 50°C min^{-1};
5. Isothermal—the temperature was maintained at the isothermal crystallization temperature (T_1, T_2, T_3, T_4, or $T_{5)}$ for 90 min;
6. Temperature scan—the sample was heated from the isothermal crystallization temperature (T_1, T_2, T_3, T_4, or $T_{5)}$ to 190°C at a rate of 5°C min^{-1}.

RESULTS AND DISSCUSSION

PLLA/*o*-MMT nanocomposites

The structure of the nanocomposite in the nanometer scale has typically been established using XRD patterns and TEM observation. XRD was used to determine the distribution of MMT in the PLLA. Figure 1 represents the XRD spectra of *o*-MMT and a series of PLLA/*o*-MMT nanocomposites (2–10 wt %). The 2θ diffraction peak of the $d_{(001)}$ facet of *o*-MMT was at 4°, revealing that the distance between the interlayers was 2.5 nm. However, the characteristic 2θ (4°) which observed in pure organophilic clay disappeared in the PLLA/*o*-MMT nanocomposite, suggesting that the clay nanolayers has completely exfoliated in the polymer chain of PLLA. Figure 2 displays a TEM micrograph of a cross section of the PLLA/*o*-MMT nanocomposite that incorporates 10 wt % *o*-MMT. At 50,000× magnification, the *o*-MMT units appeared to be uniformly distributed within the PLLA. XRD patterns and TEM observation established that exfoliated nanocomposites were formed in the PLLA/*o*-MMT.[31–33]

DSC analysis

Nonisothermal crystallization

DSC analysis was performed to determine the crystallization temperature (T_c), crystallization time, and melting point (T_m) from the exothermic peak of the samples that were prepared under nonisothermal crystallization conditions. Figure 3 shows cooling curves of the neat PLLA and PLLA/*o*-MMT nanocomposites (2–10 wt %) that were obtained at a cooling rate of 1°C min^{-1}. The neat PLLA yielded no obvious peak; hence it was amorphous under nonisothermal crystallization conditions. However, the peak of the PLLA/*o*-MMT nanocomposites (2–10 wt %) was narrow and sharp. Increasing the amount of *o*-MMT in PLLA from 2 to 10 wt % raised the crystallization temperature (from 113.4 to 114.9°C) and reduced the crystallization time (from 25 to 15 min). The dispersed *o*-MMT particles act as an effective nucleating agent, causing higher crystallization temperature and less crystallization time.

Figure 4 was plotted to show the heating curves of neat PLLA and PLLA/*o*-MMT nanocomposites (2–10 wt %) obtained at a heating rate of 5°C min^{-1}. The curves of the PLLA/*o*-MMT nanocomposites (2–10 wt %) included two endothermic peaks, but that of the neat PLLA included only one. The temperature of the lower-temperature endothermic peak (T_{m1}) decreased as the *o*-MMT content increased, with values of 168.3, 167.2, 166.9, 166.4, 166.2, and 166.6°C at 0, 2, 4, 6, 8, and 10 wt %, respectively. The presence of a higher-temperature endothermic peak (T_{m2}) at $\sim$ 171.5°C indicates that the melted crystal had recrystallized to form a more perfect crystal, which underwent fusion again as the heating temperature of the DSC instrument was increased. We can conclude that the recrystallizaion occurs in the PLLA/*o*-MMT nanocomposites that incorporated organophilic MMT under nonisothermal crystallization condition.

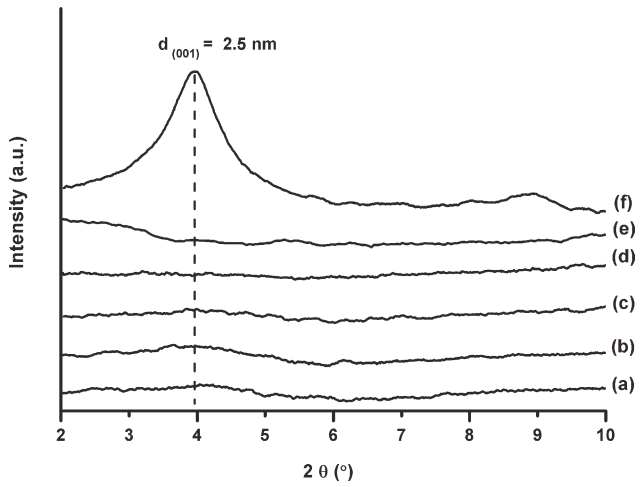

Figure 1 The XRD spectra of *o*-MMT and a series of PLLA/*o*-MMT nanocomposites (2–10 wt %). (a) 2 wt %, (b) 4 wt %, (c) 6 wt %, (d) 8 wt %, (e) 10 wt %, (f) *o*-MMT.

Isothermal crystallization

The upper cooling curves obtained by DSC under nonisothermal crystallization conditions were utilized to determine the isothermal crystallization temperature (T_1, T_2, T_3, T_4, or $T_{5)}$ of the samples. The isothermal crystallization temperatures of the PLLA/*o*-MMT nanocomposites (as shown in Table I) decreased as the *o*-MMT content increased.

Figure 2 TEM micrograph (×50,000) of the PLLA/*o*-MMT nanocomposite incorporating 10 wt % MMT.

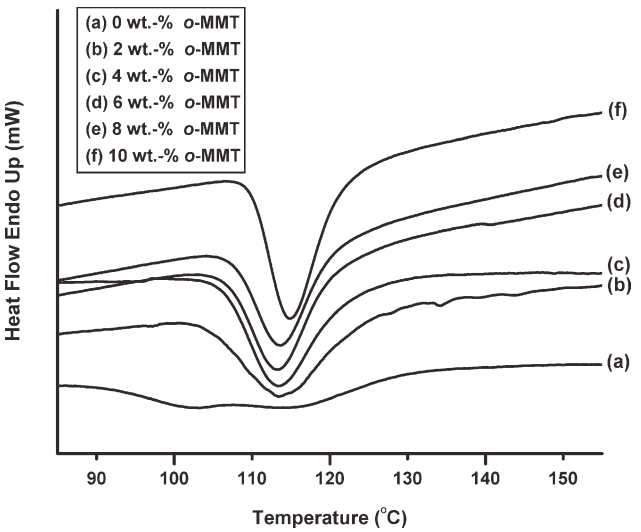

Figure 3 DSC thermograms (cooling scan) of (a–f) PLLA/*o*-MMT nanocomposites incorporating 0, 2, 4, 6, 8, and 10 wt % MMT (scan range: 25–190°C; scan rate: 1°C min^{-1}).

Figure 5 shows the cooling curves of the PLLA/4 wt % *o*-MMT nanocomposites that were prepared at various isothermal crystallization temperatures. The peak became broader, indicating that the crystallization time of the PLLA/*o*-MMT nanocomposites increased (from 17 to 48 min), corresponding to a greater enthalpy of crystallization as the crystallization temperature increased (T_c, from 117.2 to 131.1°C). This was presumably because that as the

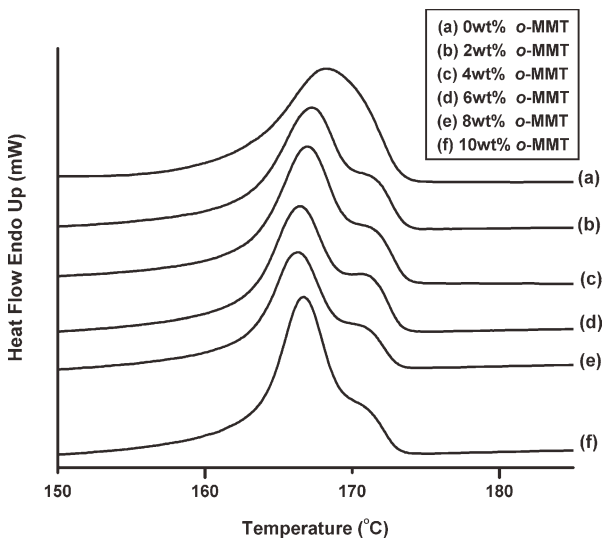

Figure 4 DSC thermograms (second heating scan) of (a–f) PLLA/*o*-MMT nanocomposites incorporating 0, 2, 4, 6, 8, and 10 wt % *o*-MMT (scan range: 25–190°C; scan rate: 5°C min^{-1}).

TABLE I
The Crystallization Temperature (T_c) of the PLLA and PLLA/*o*-MMT Nanocomposites Prepared at Isothermal Crystallization Condition

o-MMT content (wt %)	T_c (°C)				
	T_1	T_2	T_3	T_4	T_5
0	120.3	124.1	128.0	131.9	135.8
2	117.8	121.8	125.7	128.8	132.5
4	117.2	121.0	124.5	127.9	131.1
6	117.1	120.5	123.9	127.3	130.6
8	116.0	119.3	122.7	126.1	129.7
10	116.1	119.3	122.5	125.6	128.8

bulk crystallization rate became more slowly and the crystallites within the spherulites became more regular, growing in radial direction as the isothermal crystallization temperature increased. Table II summarizes the total enthalpies of crystallization (ΔH_c) and crystallization times of the test samples (0–10 wt %) that were prepared at various isothermal crystallization temperatures. The crystallization time shortened as the crystallization temperature decreased and the *o*-MMT content increased, i.e., the bulk crystallization rate was affected by the crystallization temperature and the nucleating agent (*o*-MMT) content.

Figure 6 shows the heating curves of PLLA/10 wt % *o*-MMT nanocomposites that had been subjected to isothermal crystallization at various temperatures. The curves of the sample that was prepared by isothermal crystallization at T_1 and T_2 (116.1 and 119.3°C) included two endothermic peaks, but the curve of the sample that was formed at T_3, T_4, and T_5 (122.5, 125.6, and 128.8°C) included only one endothermic. A higher-temperature endothermic peak (T_{m2}) indicates recrystallization to form a more

TABLE II
The Total Enthalpies of Crystallization (ΔH_c) and Crystallization Time of the Test Samples Prepared at Various Isothermal Crystallization Temperatures

o-MMT content (wt %)		Crystallization temperature (T_c)				
		T_1	T_2	T_3	T_4	T_5
0	ΔH_c (J g^{-1})	30.81	33.29	32.95	35.99	48.93
	Time (min)	50	52	55	67	75
2	ΔH_c (J g^{-1})	31.28	33.16	34.73	35.14	35.63
	Time (min)	20	25	35	42	55
4	ΔH_c (J g^{-1})	31.33	33.05	33.85	33.96	35.23
	Time (min)	17	21	28	39	48
6	ΔH_c (J g^{-1})	31.03	31.82	32.89	33.39	33.95
	Time (min)	14	20	24	36	44
8	ΔH_c (J g^{-1})	27.81	29.92	30.24	30.35	30.66
	Time (min)	13	14	22	28	38
10	ΔH_c (J g^{-1})	31.13	32.92	33.34	34.42	34.58
	Time (min)	11	12	18	26	32

perfect crystal, which occurred at the lowest isothermal crystallization temperature (T_1). Table III represents the total enthalpies of fusion (ΔH_f) and the temperatures of the endothermic peaks of the test samples (0–10 wt %) that were prepared at various isothermal crystallization temperatures. The degree of crystallinity, χ_c, can be calculated by the following equation:

$$\chi_c = \frac{\Delta H_f}{(1-\phi)\Delta H^*} \times 100\%$$

where ΔH_f is the heat of fusion, ΔH^* denotes heat of fusion for an infinitely large crystal, and ϕ is the weight fraction of the filler in nanocomposite. ΔH^*

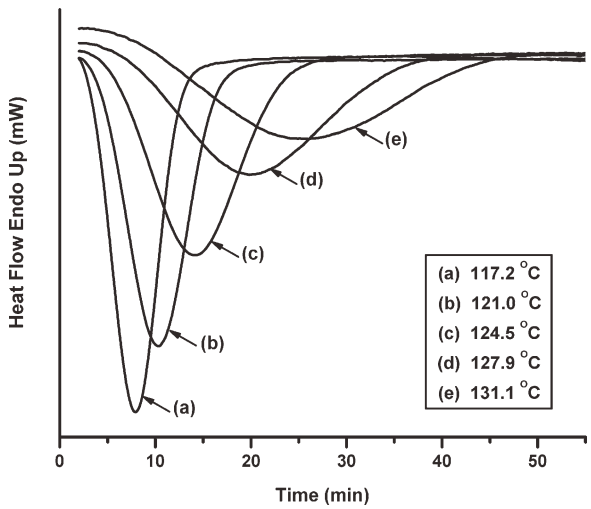

Figure 5 DSC thermograms (cooling scan) of PLLA/4 wt % *o*-MMT nanocomposites prepared at various crystallization temperatures (scan range: 25–190°C; scan rate: 1°C min^{-1}).

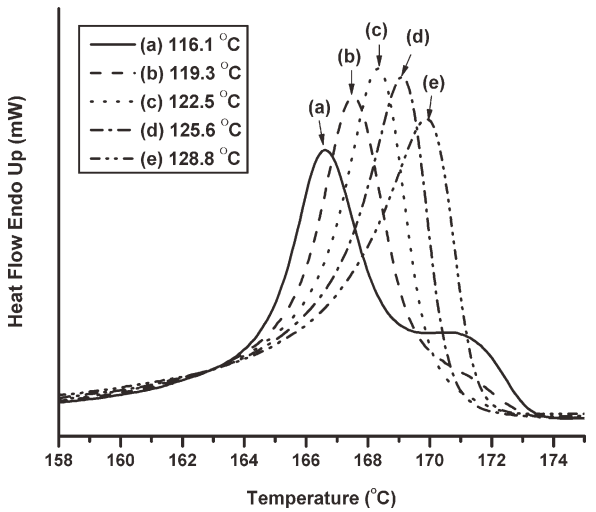

Figure 6 DSC thermograms (second heating scan) of PLLA/10 wt % *o*-MMT nanocomposites prepared at various crystallization temperatures (scan range: 25–190°C; scan rate: 5°C min^{-1}).

TABLE III
The Enthalpies of Fusion (ΔH_f) and Endothermic Peaks of the Test Samples Prepared at Various Isothermal Crystallization Temperatures

o-MMT content (wt %)		Crystallization temperature (T_c)				
		T_1	T_2	T_3	T_4	T_5
0	ΔH_f (J g^{-1})	30.71	33.62	34.21	35.93	48.61
	T_{m1} (°C)	**168.3**	**169.2**	**170.2**	**171.1**	**172.2**
	T_{m2} (°C)	–	–	–	–	–
2	ΔH_f (J g^{-1})	31.19	33.06	33.57	34.69	35.49
	T_{m1} (°C)	**167.6**	**168.5**	**169.4**	**170.1**	**171.0**
	T_{m2} (°C)	*	–	–	–	–
4	ΔH_f (J g^{-1})	31.23	33.01	33.72	33.99	35.23
	T_{m1} (°C)	**167.1**	**168.1**	**168.9**	**169.7**	**170.6**
	T_{m2} (°C)	**171.3**	*	–	–	–
6	ΔH_f (J g^{-1})	30.68	31.62	32.19	33.27	34.86
	T_{m1} (°C)	**167.2**	**168.1**	**168.9**	**169.7**	**170.5**
	T_{m2} (°C)	**171.4**	*	–	–	–
8	ΔH_f (J g^{-1})	28.08	28.64	29.55	31.61	31.79
	T_{m1} (°C)	**166.4**	**167.3**	**168.1**	**169.0**	**170.1**
	T_{m2} (°C)	**171.0**	*	–	–	–
10	ΔH_f (J g^{-1})	31.15	31.57	32.03	32.05	32.71
	T_{m1} (°C)	**166.6**	**167.5**	**168.3**	**169.1**	**169.9**
	T_{m2} (°C)	**171.3**	*	–	–	–

* = no obvious peak; –= no peak.

of PLLA was assumed 93 J g^{-1} according to the literature.[34]

The degree of crystallinity is shown as a function of crystallization temperature for PLLA/*o*-MMT nanocomposites and neat PLLA (Fig. 7). Regardless of *o*-MMT content, the crystallinity of all samples increased as the isothermal crystallization temperature, indicating that the bulk crystallization rate reduced at higher T_c, resulting in a higher overall degree of crystallinity. Moreover, in the case of nanocomposites, crystallinity is slightly higher as compared to the neat PLLA under the same isothermal crystallization temperature in the range of 116–132°C. The overall degree of crystallinity of all test samples in this study was between the ranges of 30–36%. This observation indicates that the addition of clay had no significant effect on the overall degree of crystallinity of the PLLA under the experimental condition, even when it was at higher isothermal crystallization temperature (124–132°C).

Figure 8 represents a second heating scan of the PLLA/*o*-MMT nanocomposites that incorporated 2, 4, 6, 8, and 10 wt % *o*-MMT and was prepared at crystallization temperature T_1. The PLLA that incorporated *o*-MMT under isothermal crystallization at T_1 yielded two endothermic peaks. The temperature of the lower-temperature endothermic peak (T_{m1}) decreased as the *o*-MMT content increased (0–8 wt %). But when the *o*-MMT content was over 10 wt %, the temperature increased. We suggest that excessive use of *o*-MMT caused high rigidity, influencing not only the morphology of the PLLA/*o*-MMT nanocomposites, but also promoting block melting behavior.[35,36] Additionally, the endothermic peak (T_{m2}) was at around 171°C and its intensity was proportional to the *o*-MMT content. This is presumably because the higher nucleating agent (*o*-MMT) content under lower crystallization temperature, the faster the PLLA crystallization. But the crystals produced in such a process were relatively defective. On the other hand, when the heating temperature of the DSC instrument increased, the consequent formation of crystals became more perfect. The peak (T_{m2}) disappeared, however, when the samples were

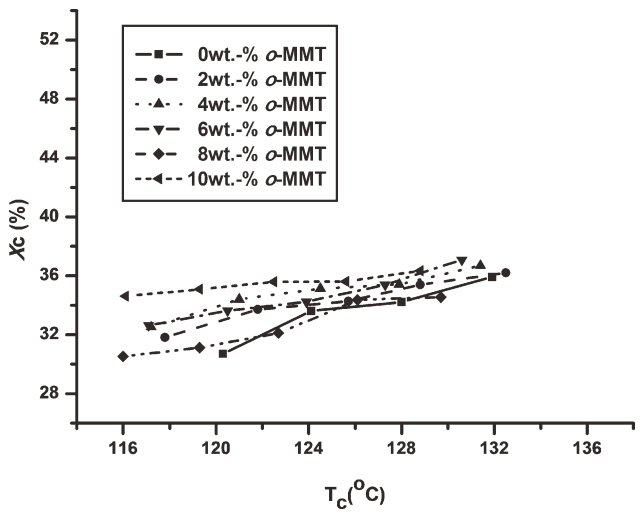

Figure 7 The degree of crystalinity as a function of crystallization temperature for PLLA/*o*-MMT nanocomposites incorporating 2, 4, 6, 8, and 10 wt % *o*-MMT, and neat PLLA.

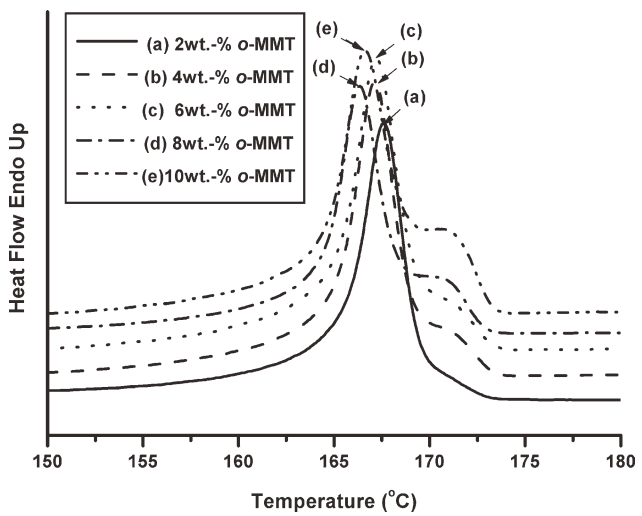

Figure 8 DSC thermograms (second heating scan) of (a–e) PLLA/*o*-MMT nanocomposites incorporating 2, 4, 6, 8, and 10 wt % *o*-MMT prepared at crystallization temperatures T_1.

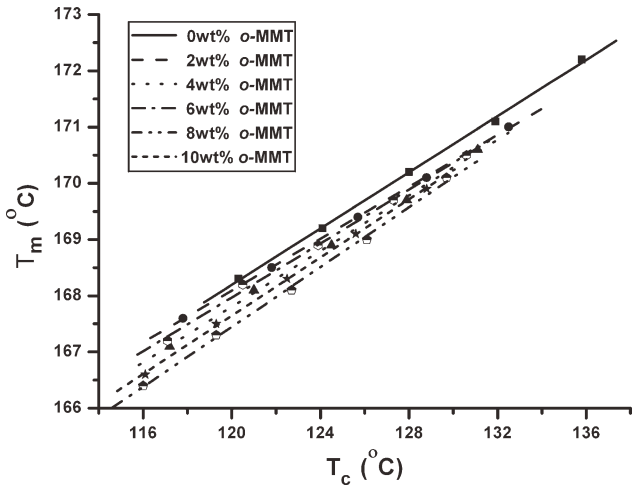

Figure 9 Variation in the T_m of the test samples with respect to the isothermal crystallization (T_c).

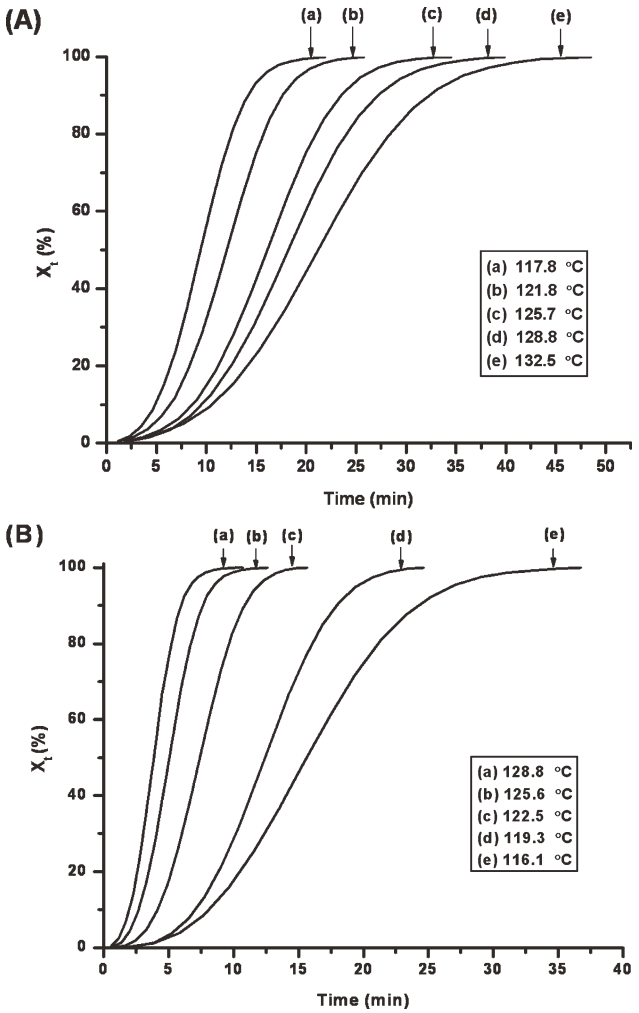

Figure 10 The variation in relative crystallinity X_t (%) of the PLLA/*o*-MMT nanocomposites with respect to the time at various isothermal crystallization temperatures (T_1–T_5) (A) 2, (B) 10 wt % *o*-MMT.

prepared at a higher crystallization temperature (T_3, T_4, T_5), even if the *o*-MMT content was increased to 10 wt %, as shown in Table III. The tendencies of changes in T_{m1} and T_{m2} at lower crystallization temperature (T_1) were similar to those under nonisothermal crystallization conditions (Fig. 4) i.e., the phenomenon of recrystallization could occur.

Figure 9 represents the variation of the melting points (T_m) in the test samples with respect to the temperature of isothermal crystallization (T_c). The results revealed that the melting point of neat PLLA and the nanocomposites became higher by increasing the isothermal crystallization temperature (T_c), indicating that the perfection and thickness of the growing PLLA lamella crystals increased at higher T_c's. As shown in Figure 9, the melting points (T_m) of the nanocomposites are lower than neat PLLA, suggesting that they produced thinner lamella crystals or defective crystalline regions. The melting points of 2–10 wt % PLLA/*o*-MMT nanocomposite almost overlapped at around 132°C. These results revealed that the independence of the melting points of the PLLA/*o*-MMT nanocomposites on the *o*-MMT content at higher isothermal crystallization temperature (>132°C).

Analysis of kinetics of crystallization

A series of isothermal crystallization data from DSC were calculated to determine the relative crystallinity (X_t) of PLLA/*o*-MMT nanocomposites and then the Avrami equation was applied to determine the dimensions of crystal growth and the rate constant of crystallization. The relative crystallinity was calculated using the following equation.

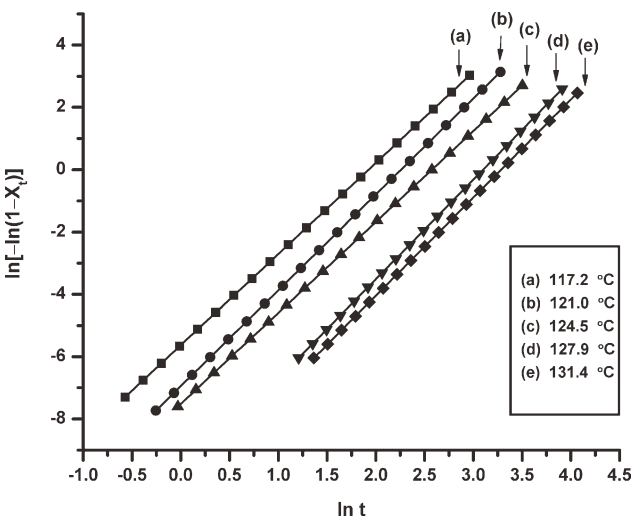

Figure 11 The linear relation of ln{−ln[1 − X_t]} and lnt for PLLA/4 wt % *o*-MMT nanocomposite at various isothermal crystallization temperatures (T_1–T_5).

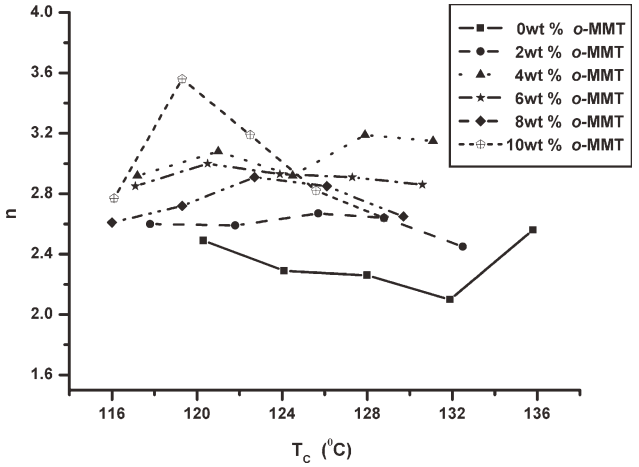

Figure 12 The *n* value of the PLLA/*o*-MMT nanocomposites (0–10 wt %) with respect to the isothermal crystallization temperature.

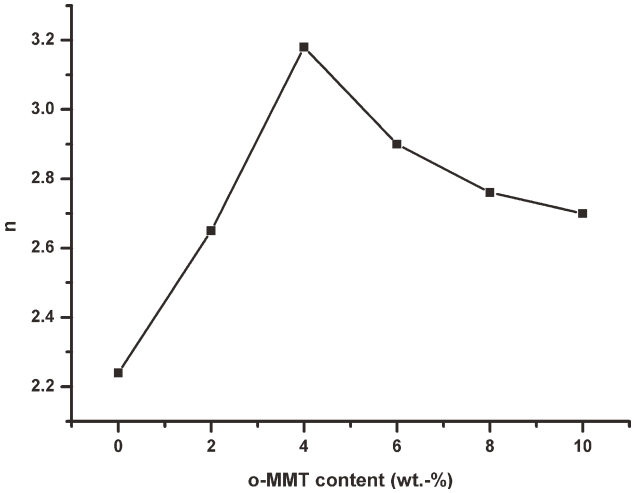

Figure 13 The value of *n* of the test sample with respect to the *o*-MMT content at crystallization temperatures 128°C.

$$X_t = \frac{\int_{T_0}^{T} (dH_c/dT)dT}{\int_{T_0}^{T\infty} (dH_c/dT)dT} \quad (2)$$

where the denominator is the total area under the isothermal crystallization graph of the PLLA/*o*-MMT nanocomposites obtained by DSC analysis, and the numerator is the area within the time range (T_0–T) in the same graph. Figure 10 shows the variation of the relative crystallinity X_t (%) of the PLLA/*o*-MMT nanocomposites (2 and 10 wt % *o*-MMT) with time (min) at various isothermal crystallization temperatures (T_1–T_5). The curves all had *S*-like shapes and were linear from 10 to 90% in the *S*-like regions. A greater slope of the linear portion represented a higher rate of crystallization. The results show that the rate of crystallization declined as the isothermal crystallization temperature increased. A comparison of Figure 10(A,B) reveals that for a given same X_t (10%), the crystallization times of PLLA/2 wt % *o*-MMT nanocomposites and PLLA/10 wt % *o*-MMT nanocomposites, prepared at T_5, were 11 and 8 min, respectively, presumably because the dominant mechanism of crystallization was nucleation at initial crystallization. Therefore, a greater amount of *o*-MMT, a nucleant, was associated with faster crystallization.

The Avrami equation is commonly not only to determine the growing rate of a metal crystal but also to analyze the crystallization rate of polymer.[37–39] This investigation studies the bulk crystallization kinetics, using the following Avrami equation.

$$1 - X_t = \exp(-k\,t^n) \quad (3)$$

where k is the crystallization rate constant and n is the Avrami exponent whose value is related to the mechanism of nucleation and the form of crystal growth. The Avrami eq. (3) can be linearized as follows.

$$\ln[-\ln(1 - X_t)] = \ln k + n \ln t \quad (4)$$

Plotting $\ln[-\ln(1 - X_t)]$ versus lnt therefore yields a straight line with a slope of n, and the value of k can be determined from the point of intersection with the y axis. Figure 11 shows the linear relation between $\ln[-\ln(1 - X_t)]$ and $\ln t$ for PLLA/4 wt % *o*-MMT nanocomposite at various isothermal crystallization temperatures (T_1–T_5). Figure 12 shows the n value of the PLLA/*o*-MMT nanocomposites

TABLE IV
The Value of *k* in the Avrami Equation of the PLLA/*o*-MMT Nanocomposites (0–10 wt %) Prepared at Various Isothermal Crystallization Temperatures (T_1–T_5)

Crystallization temperature (°C)	*o*-MMT content (wt %)					
	0	2	4	6	8	10
T_1	3.46×10^{-4}	2.15×10^{-3}	3.59×10^{-3}	3.34×10^{-3}	9.39×10^{-3}	1.82×10^{-2}
T_2	6.28×10^{-4}	1.24×10^{-3}	9.59×10^{-4}	1.07×10^{-3}	3.12×10^{-3}	6.85×10^{-3}
T_3	2.86×10^{-4}	4.65×10^{-4}	5.45×10^{-4}	4.97×10^{-4}	9.52×10^{-4}	1.15×10^{-3}
T_4	4.16×10^{-4}	3.52×10^{-4}	5.00×10^{-5}	1.64×10^{-4}	4.51×10^{-4}	3.29×10^{-4}
T_5	4.80×10^{-5}	4.42×10^{-4}	3.23×10^{-5}	1.29×10^{-4}	3.79×10^{-4}	8.50×10^{-5}

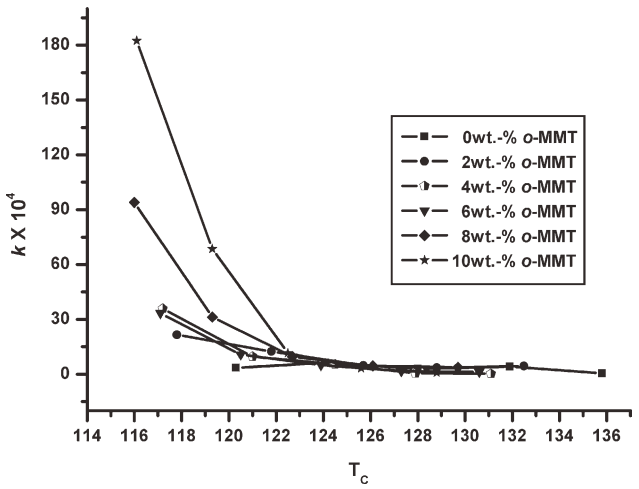

Figure 14 The k value of the PLLA/*o*-MMT nanocomposites (0–10 wt %) with respect to the isothermal crystallization temperature.

(0–10 wt %) versus the isothermal crystallization temperature. A remarkable difference between neat PLLA and PLLA/*o*-MMT nanocomposites was observed: the increase in n upon the addition of *o*-MMT reveals that *o*-MMT induced crystallization of the PLLA/*o*-MMT nanocomposites. The n value of neat PLLA was around 2.10–2.56 and those of the PLLA/*o*-MMT (4–8 wt %) nanocomposites were around 2.61–3.19. The Avrami exponent (n) represents the dimensionality of the growth, which was higher in all of the PLLA/*o*-MMT nanocomposites compared with neat PLLA. When $n = 3$, they formed spherical growth; $n = 2$, circular disk shape growth.[40] Therefore, the observed n values from PLLA/*o*-MMT nanocomposites closed to 3, suggesting that well-defined spherulitic structures can be obtained by loading *o*-MMT. Moreover, Figure 13 displays the variation in the values of n in the test samples with respect to the *o*-MMT content at 128°C. The n value increased by increasing *o*-MMT content up to 4 wt %, and then it started to decrease by further increasing the *o*-MMT content. The n value of neat PLLA is 2.24, signifying the spherulite growth of neat PLLA is almost a circular disk shape. On the other hand, on the basis of Figure 13, higher *o*-MMT content (>4 wt %) hindered the chain-folding mechanism needed for local PLLA crystallization, resulting in the decreased n value.

Table IV summarizes the value k of the test samples (0–10 wt %) that were prepared at various isothermal crystallization temperatures (T_1–T_5). Figure 14 shows k value of the PLLA/*o*-MMT nanocomposites (0–10 wt %) versus the isothermal crystallization temperature. The k value decreased significantly with the isothermal crystallization temperature (<123°C) and increased with the *o*-MMT content for all test samples. The crystallization rate was determined by the nucleation rate of crystallization i.e., by the amount of *o*-MMT (nucleant) at low crystallization temperatures.

A larger k value was corresponding to a higher rate of crystallization. Table IV shows that adding *o*-MMT in PLLA accelerated crystallization. This finding was consistent with the results of the crystallization and crystallization time, which involved DSC analysis. The k values of the test samples were similar to one another when the crystallization temperature exceeded 123°C.

Crystallization half-time,$t_{1/2}$, is defined as the time at which the extent of crystallization reaches 50%. It is regarded as a very important crystallization kinetics parameter. It is used to characterize the crystallization rate directly. It can be said that the longer the $t_{1/2}$, the slower the crystallization rate. The results in Table V were in accordance with those deduced from the Avrami integral curves (Fig. 10). Usually, the rate of crystallization is described as the reciprocal of $t_{1/2}$ i.e., $(t_{1/2})^{-1}$. The calculated values of $(t_{1/2})^{-1}$ were also listed in Table V. Figure 15 shows $(t_{1/2})^{-1}$ value of the PLLA/*o*-MMT nanocomposites (0–10 wt %) versus the isothermal crystallization temperature. Figure 15 indicates that the rate of crystallization of the PLLA/*o*-MMT nanocomposites is significantly faster than neat PLLA under lower isothermal crystallization temperature, implying that the clay acts as an effective nucleating agent. Hence

TABLE V
Crystallization Half-Time, $t_{1/2}$, and $(t_{1/2})^{-1}$ of the PLLA/*o*-MMT Nanocomposites (0–10 wt %) Prepared at Various Isothermal Crystallization Temperatures (T_1–T_5)

	T_1		T_2		T_3		T_4		T_5	
o-MMT content (wt %)	$t_{1/2}$ (min)	$(t_{1/2})^{-1}$ $(\text{min})^{-1}$	$t_{1/2}$ (min)	$(t_{1/2})^{-1}$ $(\text{min})^{-1}$	$t_{1/2}$ (min)	$(t_{1/2})^{-1}$ $(\text{min})^{-1}$	$t_{1/2}$ (min)	$(t_{1/2})^{-1}$ $(\text{min})^{-1}$	$t_{1/2}$ (min)	$(t_{1/2})^{-1}$ $(\text{min})^{-1}$
0	20.1	0.0498	23.2	0.0431	26.3	0.0380	29.7	0.0337	38.8	0.0258
2	9.3	0.1075	12.1	0.0826	16.0	0.0625	18.2	0.0549	21.1	0.0474
4	5.9	0.1695	8.3	0.1205	11.7	0.0855	19.4	0.0515	23.6	0.0424
6	6.5	0.1538	8.5	0.1176	11.9	0.0840	18.3	0.0546	20.6	0.0485
8	5.2	0.1923	6.7	0.1493	9.8	0.1020	15.5	0.0645	18.5	0.0541
10	3.9	0.2564	5.1	0.1961	7.4	0.1351	12.4	0.0806	15.7	0.0637

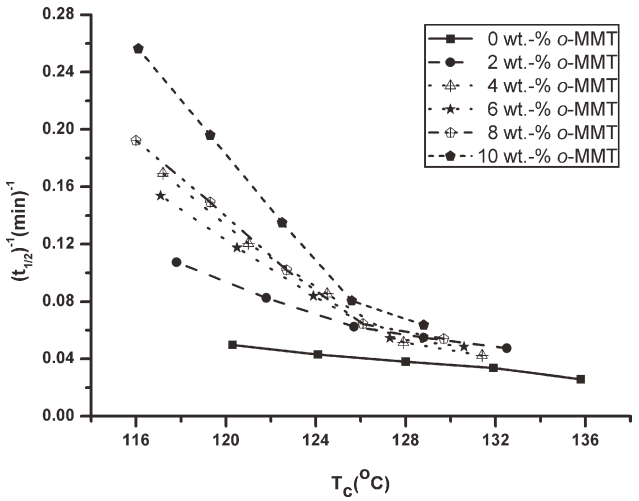

Figure 15 The $(t_{1/2})^{-1}$ value of the PLLA/*o*-MMT nanocomposites (0–10 wt %) versus the isothermal crystallization temperature.

higher nucleation density in PLLA leads to increased bulk crystallization rates. In contrast, under higher isothermal crystallization temperatures, bulk crystallization rates are critically dependent on the rate of spherulitic growth—not the rate of nucleation. The clay loading has almost no effect on the acceleration of spherulite growth rate during the crystallization of PLLA/*o*-MMT nanocomposites because the encapsulation of clay throughout the semicrystalline spherulite, resulting that the crystallization rates of PLLA/*o*-MMT nanocomposites are similar to that of neat PLLA.[41]

CONCLUSIONS

A series of PLLA/*o*-MMT nanocomposites (2–10 wt %) were prepared by solution intercalation. Organophilic MMT was exfoliated and evenly dispersed in the PLLA matrix. The DSC thermal curve demonstrates that the incorporation of *o*-MMT into the PLLA yields two endothermic peaks at nonisothermal temperatures, which are not obtained from neat-PLLA, suggesting recrystallization. Moreover, the recrystallization of PLLA/*o*-MMT nanocomposites was evidently observed when they were both isothermally crystallized at low temperatures (T_1) and the *o*-MMT content over 2 wt %, which can be attributed to the fact that the bulk crystallization rate of the PLLA/*o*-MMT nanocomposites was faster at lower crystallization temperature (T_1) and less crystal perfection. This is further evidence that the melting point of the nanocomposites significantly decreases by decreasing the isothermal crystallization temperature (T_c). The *o*-MMT incorporation within PLLA has slightly increased the overall degree of crystallinity from 30 to 36% under the experimental condition (116–132°C).

Avrami analysis indicated that clay incorporation drove the growth geometry toward more three-dimensional (spherical growth) rather than two-dimensional (disk shaped). We found that at higher *o*-MMT loading (6–10 wt %), the dispersed clay platelet retarded the spherulite growth, thus greatly reduced the Avrami exponent (n) compared to PLLA/4 wt % *o*-MMT nanocomposites (from 3.18 to 2.7) at isothermal crystallization condition (128°C). In addition, based on the Avrami equation, the employment of the crystallization rate constant (k) or the reciprocal of crystallization half-time, $(t_{1/2})^{-1}$ characterized the rate of bulk crystallization. A larger k value or $(t_{1/2})^{-1}$ value is corresponding to a higher rate of bulk crystallization. We proved that the k value or $(t_{1/2})^{-1}$ value of the PLLA/*o*-MMT nanocomposites is higher than that of neat PLLA. The k value or $(t_{1/2})^{-1}$ value of the PLLA/*o*-MMT nanocomposites increased considerably with the *o*-MMT content under the lower isothermal crystallization temperature (<123°C), while it increased slightly with the *o*-MMT content under the higher isothermal crystallization temperatures. This phenomenon implies that the *o*-MMT acts as an effective nucleating agent, especially under the lower isothermal crystallization temperature.

The results presented herein suggest that one can produce the final physical and mechanical properties of PLLA nanocomposite materials by incorporating various contents of *o*-MMT under various isothermal crystallization condition, tuning degree of crystallinity, the content of nucleating agent, the crystallization rate, and the ultimate crystallization morphology.

References

1. Hoogsteen, W.; Postema, A. R.; Pennings, A. J.; Brinke, G. T.; Zugenmaier, P. Macromolecules 1990, 23, 634.
2. Alemán, C.; Lotz, B.; Puiggali, J. Macromolecules 2001, 34, 4795.
3. Cartiera, L.; Okihara, T.; Ikada, Y.; Tsuji, H.; Puiggali, J.; Lotz, B. Polymer 2000, 41, 8909.
4. Puiggali, J.; Ikada, Y.; Tsuji, H.; Cartier, L.; Okihara, T.; Lotz, B. Polymer 2000, 41, 8921.
5. Okada, A.; Usuki, A.; Kurauchi, T.; Kamigaito, O. ACS Symp Series 1995, 55, 585.
6. Moet Akelah, A. J Appl Polym Sci Appl Polym Symp 1994, 55, 153.
7. Pinnavaia, T.; Beall, G. W. Polymer-Clay Nanocomposites; Wiley: New York, 2000; Chapter 3.
8. Ke, Y.; Long, C.; Qi, Z. J Appl Polym Sci 1999, 71, 1139.
9. Su, S.; Wilkie, C. A. J Polym Sci A Polym Chem 2003, 41, 1124.
10. Messersmith, P. B.; Giannelis, E. P. J Polym Sci A Polym Chem 1995, 33, 1047.
11. Gorrasi, G.; Tortora, M.; Vittoria, V. J Polym Sci B Polym Phys 2005, 43, 2454.
12. Ni, P.; Li, J.; Suo, J.; Li, S. J Appl Polym Sci 2004, 94, 534.
13. Goda, H.; Frank, C. W. Chem Mater 2001, 13, 2783.
14. Chang, J. H.; An, Y. U. J Polym Sci B Polym Phys 2002, 40, 670.

15. Lee, M. H.; Dan, C. H.; Kim, J. H.; Cha, J.; Kim, S.; Hwang, Y.; Lee, C. H. Polymer 2006, 47, 4359.
16. Weon, J. I.; Sue, H. J. Polymer 2005, 46, 6325.
17. Xu, Y.; Hoa, S. V. Compos Sci Technol 2008, 68, 854.
18. Balakrishnan, S.; Start, P. R.; Raghavan, D.; Hudson, S. D. Polymer 2005, 46, 11255.
19. Agag, T.; Koga, T.; Takeichi, T. Polymer 2001, 42, 3399.
20. Delozier, D. M.; Orwoll, R. A.; Cahoon, J. F.; Johnston, N. J.; Smith, J. G.; Connell, J. W. Polymer 2002, 43, 813.
21. Park, C.; Smith, J. G.; Connell, J. W.; Lowther, S. E.; Working, D. C.; Siochi, E. J. Polymer 2005, 46, 9694.
22. Yano, K.; Usuki, A.; Okada, A.; Kurauchi, T.; Kamigaito, O. Polym Prepr (Jpn) 1991, 32, 65.
23. Usuki, A.; Kojima, Y.; Kawasumi, M.; Okada, A.; Fukushima, Y.; Kurauchi, T.; Kamigaito, O. J Mater Res 1993, 8, 1179.
24. Vaia, R. A.; Giannelis, E. P. Macromolecules 1997, 30, 7990.
25. Alexandre, M.; Dubois, P. Mater Sci Eng 2000, 28, 1.
26. Kojima, Y.; Usuki, A.; Kawasumi, M.; Okada, A.; Fukushima, Y.; Kurauchi, T.; Kamigaito, O. J Mater Res 1993, 8, 1185.
27. Fukushima, Y.; Okada, A.; Kawasumi, M.; Kurauchi, T.; Kamigaito, O. Clay Miner 1988, 23, 27.
28. Usuki, A.; Kawasumi, M.; Kojima, Y.; Okada, A.; Kurauchi, T.; Kamigaito, O. J Mater Res 1993, 8, 1174.
29. LeBaron, P. C.; Wang, Z.; Pinnavaia, T. J. Appl Clay Sci 1999, 15, 11.
30. Huang, S. M.; Hwang, J. J.; Liu, H. J.; Lin, L. H. J Appl Polym Sci 2010, 117, 434.
31. Navarchian, A. H.; Majdzadeh-Ardakani, K. J Appl Polym Sci 2009, 114, 531.
32. Ozkoc, G.; Kemaloglu, S. J Appl Polym Sci 2009, 114, 2481.
33. Miyagawa, H.; Rich, M. J.; Drzal, L. T. J Polym Sci B Polym Phys 2004, 42, 4384.
34. Fischer, E. W.; Sterzel, H. J.; Wegner, G.; Kolloid, Z. Z. Polymer 1973, 251, 980.
35. Ray, S. S.; Okamoto, M. Prog Polym Sci 2003, 28, 1539.
36. Pluta, M. Polymer 2004, 45, 8239.
37. Avrami, M. J Chem Phys 1939, 7, 1130.
38. Avrami, M. J Chem Phys 1940, 8, 212.
39. Avrami, M. J Chem Phys 1941, 9, 177.
40. Schultz, J. M. Polymer Crystallization: The Development of Crystalline Order in Thermoplastic Polymers; Oxford University Press: New York, 2001.
41. Vahik, K.; Pochan, D. J. Macromolecules 2004, 37, 6480.